The Iranian Journal of Mechanical Engineering Transactions of ISME
Journal homepage: https://jmee.isme.ir/
Vol. 26, No. 1, 2025, pp. 44-65

Research Paper

DOI: https://doi.org/10.30506/jmee.2024.2036583.1350

Fracture Behavior of Bonded Dissimilar Piezoelectric Rectangular Planes with Multiple Interfacial Cracks under Anti-plane Mechanical and In-plane Electric Impact Loads

Mojtaba Ayatollahi[*]
Professor

Reza Teymoori Faal[†]
Professor

Mohsen Shirnezhad[‡]
M.Sc. Student

The paper aims to investigate the problem of interfacial cracks in two bonded dissimilar piezoelectric rectangular planes. First, we solve the problem of dynamic electro-elastic dislocation in a piezoelectric two-layer rectangle and conduct an asymptotic analysis of the stress and electric displacement. Then, the problem is formulated as a system of singular integral equations in the Laplace transform domain. The dislocation density functions on the crack surface are determined by solving singular integral equations numerically. The dynamic mechanical and electrical field intensity factors are calculated for various crack geometries, loading parameters, and different rectangular piezoelectric materials. The numerical results show that the material properties of bonded planes have a significant impact on the peak and steady values of the field intensity factors. Furthermore, the influence of the dimensions of the rectangular plane, as well as the sign and magnitude of the loading parameter on the field intensity factors, is discussed.

Keywords: Dissimilar rectangular piezoelectric planes, Dynamic electro-elastic dislocation, Electro-mechanical impacts, Interfacial cracks, Field intensity factor

1 Introduction

Piezoelectricity allows the conversion of electricity into acoustic signals. By using a piezoelectric crystal, it is possible to accurately generate the required quantities of electric charges.

[*]Corresponding author, Professor, Faculty of Engineering, University of Zanjan, Zanjan, Iran, mo_ayatollahi@znu.ac.ir
[†] Professor, Faculty of Engineering, University of Zanjan, Zanjan, Iran, reza.faal@znu.ac.ir
[‡] M.Sc. Student, Faculty of Engineering, University of Zanjan, Zanjan, Iran, mohsenshirnezhad@gmail.com

Received: 2024/07/24, Revised: 2024/08/15, Accepted: 2024/09/01

This is needed in the construction of precision electrometers. Such devices were used for the measurement of capacitance, voltage, pyroelectric, and piezoelectric effects and in the measurements of radioactivity. Furthermore, piezoelectric sensors have been more widely used in precision instrumentation, manufacturing, and mechatronics for measuring pressure, vibrations, stress, strain, and acceleration, as well as impact detectors, and position sensors. It is widely accepted that piezoelectric composites have low toughness and are highly brittle in commercial use. Therefore, it may be necessary to study how cracked composite smart structures respond to electro-mechanical impacts.Consequently, a comprehensive understanding of the failure mechanism of these composite materials under impact loads has become an exciting research topic for the research community [1-8].

The review content can be categorized into four main groups. Therefore, the first part of the literature review is devoted to articles that directly solve crack problems in elastic plates without providing fundamental solutions such as dislocation solutions. The out-of-plane deformation of a rectangular orthotropic plate with a crack was examined by Chang [9]. In this study, the integral transform was used and the stress intensity factor was obtained. Ma [10] investigated the solution of a rectangular sheet that was clamped and weakened by a crack located on the line of symmetry of the plane. A study was conducted by Zhang [11] on a finite rectangular plate containing two interacting edge cracks under the SH shear wave. In another work, Ma and Zhang [12] solved the problem of an eccentric crack in a rectangular plane subjected to anti-plane shear. Mirzaei et al. [13] presented an approximate solution for the stress and displacement fields around the blunt notches in bi-material media under in-plane loading. Bahrami et al. [14] obtained the stress field in adhesively bonded joints by employing an analytical approach together with the finite element method (FEM). The review's second part discussed the cracked piezoelectric rectangular plane but did not find Green’s function solution to the problem. Li and Lee [15] obtained the mode III stress intensity factor for an arbitrarily oriented crack in a rectangular piezoelectric plane. The paper by Yu et al. [16] solves the problem of an interfacial impermeable crack in dissimilar piezoelectric solids under coupled electromechanical impact loadings using the extended finite element method (X-FEM). Pamnani et al. [17], studied the impermeable crack at the interface of piezoelectric materials. The study utilized an extended finite element method to analyze an edge crack and central crack located at the interface of PZT-5H and PZT-4 piezoelectric materials. The analysis was carried out under static electro-mechanical loadings.

To our knowledge, limited efforts have been made to analyze the cracked materials with finite geometry by using the fundamental solutions. Generally, the closed-form fundamental solutions are obtained under static conditions. Furthermore, integral transform methods and the distributed dislocation technique, mainly the Fourier transform, are the most commonly used methods for deriving fundamental solutions. The third section of the literature review discussed the utilization of fundamental solutions for cracked finite planes. Faal and Dehgan [18] tackled the problem of the functionally graded rectangular planes weakened by several cracks. The numerical results were given for single, two vertical, horizontal cracks, and two arc cracks. Gu et al. [19] solved the problem of cracked plates subjected to far-field tensile and shear loadings using the localized method of fundamental solutions. The anti-plane deformation of an electrically loaded rectangular piezoelectric plane with several defects was examined by Abazadeh and Darafshani [20]. The review's final section discussed the behavior of a cracked finite piezoelectric plane under impact loads. The papers on the dynamic response of finite piezoelectric bodies with cracks are limited. The investigation by Ayatollahi et al. [21] focused on transient analysis in a rectangular plane made of functionally graded magneto-electro-elastic materials and containing multiple defects under various boundary conditions. They obtained dynamic stress intensity factors (DSIFs), by employing the distributed dislocation technique with the aid of the integral transform method.

In the literature, there appears to be a lack of information on the transient behavior of bonded piezoelectric material containing interfacial cracks with finite geometry under impacts.
Hence, the objective of this paper is to develop a fundamental solution for the transient problem of two rectangular piezoelectric plates bonded together with dissimilar properties, weakened by several interfacial cracks, and under electro-mechanical impact loads. The analysis relies on the distributed dislocation technique. The main challenge is to efficiently obtain a dislocation solution for constructing the integral equations with Cauchy singularities in dynamic interfacial crack problems. The main goal of this paper is to find the fundamental solution in piezoelectric two-layer rectangles to study their dynamic fracture behavior in the vicinity of several interfacial cracks subjected to electro-mechanical impacts. To accomplish this task, numerical examples were obtained for various loading ratios, different geometry of the planes and interacting interfacial crack length.

2 Formulation of the problems

For the piezoelectric materials, by assuming a sufficiently small range of loading and a constant polarization field, we can use the generalized linear fracture mechanics concepts. Therefore, the transient response of piezoelectric bodies is determined by the equations of the linear theory of piezoelectricity. In piezoelectricity, the quasi-static electric field is interconnected with dynamic mechanical motion. The equations of linear elasticity are precisely linked to the charge equation of electrostatics through the piezoelectric constants in the absence of body force and electric charge density. The geometry of the dissimilar piezoelectric rectangular planes under consideration is shown in Fig. (1). The polarization direction of the composite medium is along *z–axis*. For the case of anti-plane deformation under the in-plane electric fields, the expressions for the components of anti-plane shear stresses and electric displacement are defined as follows:

$$\begin{aligned}
\sigma_{zx}^{(k)}(x,y,t) &= c_{44}^{(k)}\frac{\partial w^{(k)}(x,y,t)}{\partial x}+e_{15}^{(k)}\frac{\partial \varphi^{(k)}(x,y,t)}{\partial x}\\
\sigma_{zy}^{(k)}(x,y,t) &= c_{44}^{(k)}\frac{\partial w^{(k)}(x,y,t)}{\partial y}+e_{15}^{(k)}\frac{\partial \varphi^{(k)}(x,y,t)}{\partial y}\\
D_{x}^{(k)}(x,y,t) &= e_{15}^{(k)}\frac{\partial w^{(k)}(x,y,t)}{\partial x}-\varepsilon_{11}^{(k)}\frac{\partial \varphi^{(k)}(x,y,t)}{\partial x}\\
D_{y}^{(k)}(x,y,t) &= e_{15}^{(k)}\frac{\partial w^{(k)}(x,y,t)}{\partial y}-\varepsilon_{11}^{(k)}\frac{\partial \varphi^{(k)}(x,y,t)}{\partial y} \qquad k=1,2
\end{aligned} \tag{1}$$

In the usual notation $\sigma_{ij}^{(k)}$, $D_i^{(k)}$, $w^{(k)}$ and φ are stresses, electric displacements, mechanical displacements, and electric potential, respectively. $c_{44}^{(k)}$, $e_{15}^{(k)}$ and, $\varepsilon_{11}^{(k)}$ are the elastic stiffness, piezoelectric, and dielectric constants of each region, ($k=1$ for $h_2<y<h$ and $k=2$ for $0<y<h_2$, Fig. (1)).
We assume that the electric charge density and the body force are zero. By using the equations of motion and the Maxwell equations, the governing equations for bonded dissimilar rectangles may be expressed as follows [8]:

$$\begin{aligned}
c_{44}^{(k)}\nabla^2 w^{(k)}(x,y,t)+e_{15}^{(k)}\nabla^2\varphi^{(k)}(x,y,t) &= \rho^{(k)}\frac{\partial^2 w^{(k)}(x,y,t)}{\partial t^2},\\
e_{15}^{(k)}\nabla^2 w^{(k)}(x,y,t)-\varepsilon_{11}^{(k)}\nabla^2\varphi^{(k)}(x,y,t) &= 0 \qquad k=1,2
\end{aligned} \tag{2}$$

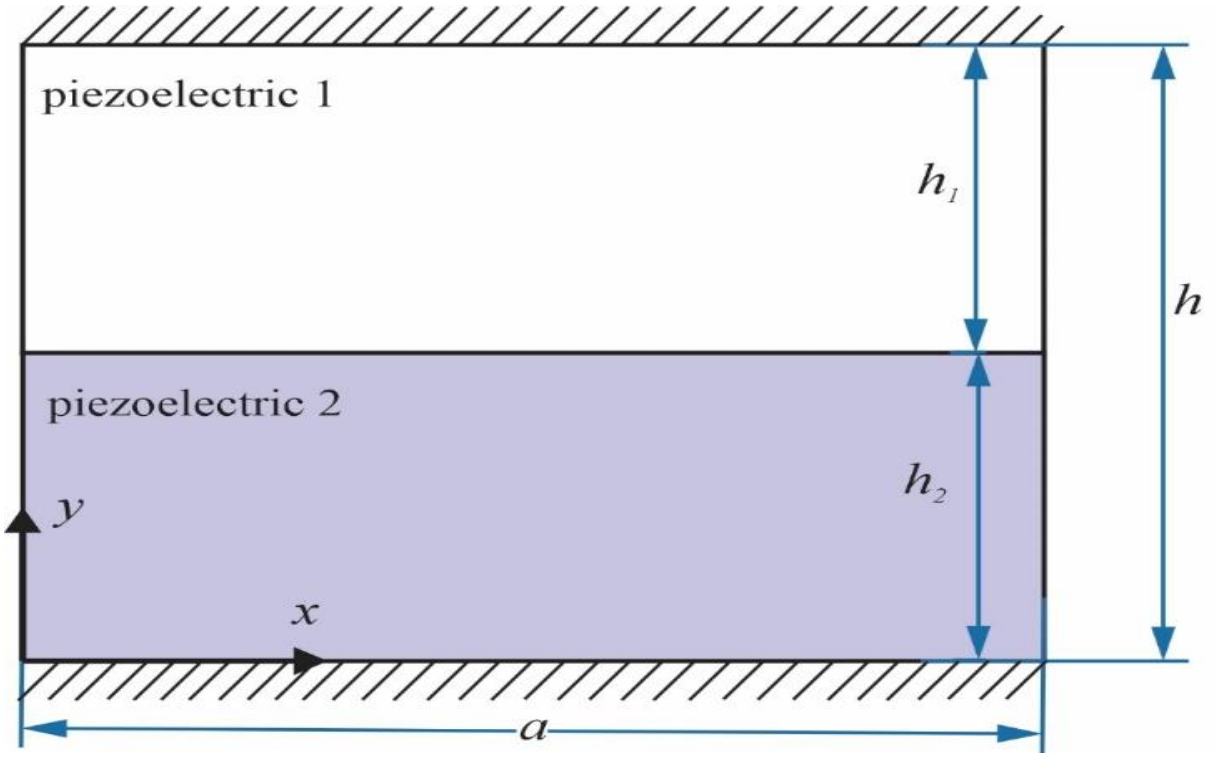

Figure1 Geometry of bonded dissimilar piezoelectric rectangles with clamped edges

From Eq. (2) it may be seen that the solution of the problem for the fields of mechanical displacement and electric potential must be obtained through the coupled equations of electroelasticity. By defining the following auxiliary functions, the governing equations may be reduced to uncoupled forms. (see, for example, [8]).

$$\varphi^{(k)}(x,y,t)=\varphi^{*(k)}(x,y,t)+\alpha^{(k)}w^{(k)}(x,y,t) \quad k=1,2 \tag{3}$$

where $\alpha^{(k)}=e_{15}^{(k)}/\varepsilon_{11}^{(k)}$, the constitutive equations (1), are rewritten as:

$$\begin{aligned}
\sigma_{zx}^{(k)}(x,y,t)&=\gamma^{(k)}\frac{\partial w^{(k)}}{\partial x}(x,y,t)+e_{15}^{(k)}\frac{\partial \varphi^{*(k)}}{\partial x}(x,y,t),\\
\sigma_{zy}^{(k)}(x,y,t)&=\gamma^{(k)}\frac{\partial w^{(k)}}{\partial y}(x,y,t)+e_{15}^{(k)}\frac{\partial \varphi^{*(k)}}{\partial y}(x,y,t),\\
D_x^{(k)}(x,y,t)&=-\varepsilon_{11}^{(k)}\frac{\partial \varphi^{*(k)}}{\partial x}(x,y,t),\\
D_y^{(k)}(x,y,t)&=-\varepsilon_{11}^{(k)}\frac{\partial \varphi^{*(k)}}{\partial y}(x,y,t) \qquad k=1,2.
\end{aligned} \tag{4}$$

where $\gamma^{(k)}=c_{44}^{(k)}+\alpha^{(k)}e_{15}^{(k)}$ is the piezoelectric constant. Substituting (3) into (2), the governing equations in terms of mechanical displacement and electric potential reduce to:

$$\begin{aligned}
\nabla^2 w^{(k)}(x,y,t)&=\frac{1}{[c_s^{(k)}]^2}\frac{\partial^2 w^{(k)}}{\partial t^2}(x,y,t),\\
\nabla^2 \varphi^{*(k)}(x,y,t)&=0 \qquad k=1,2
\end{aligned} \tag{5}$$

where $c_s^{(k)} = \sqrt{\gamma^{(k)}/\rho^{(k)}}$ is the shear wave speed. We further assumed that the initial displacement, velocity, and electric potential are zero. To obtain a solution, we introduce the following finite Fourier cosine and Laplace transforms, respectively:

$$F_c(n,y,t) = \int_0^a f(x,y,t)\cos(\frac{n\pi}{a}x)dx,$$
$$\bar{f}(x,y,s) = \int_0^\infty w(x,y,t)e^{-st}dt \tag{6}$$

where the bar indicates the Laplace transform and s is the Laplace transform Parameter. Taking finite Fourier cosine-Laplace transformations in variables x,t, and making use of the zero initial conditions, leads to:

$$\frac{d^2}{dy^2}\begin{Bmatrix}\bar{W}_c^{(k)}(n,y,s)\\ \bar{\Phi}_c^*(n,y,s)\end{Bmatrix} - \begin{Bmatrix}(\lambda_n^{(k)})^2\\ \beta_n{}^2\end{Bmatrix}\begin{Bmatrix}\bar{W}_c^{(k)}(n,y,s)\\ \bar{\Phi}_c^*(n,y,s)\end{Bmatrix} = (-1)^{n+1}\frac{d}{dx}\begin{Bmatrix}\bar{w}^{(k)}(a,y,s)\\ \bar{\varphi}(a,y,s)\end{Bmatrix} + \frac{d}{dx}\begin{Bmatrix}\bar{w}(0,y,s)\\ \bar{\varphi}(0,y,s)\end{Bmatrix}, \tag{7}$$

Where $\beta_n = (n\pi/a)$ and $\lambda_n^{(k)} = \sqrt{(\beta_n)^2 + (s/c_s^{(k)})^2}$, The homogeneous solution of the differential equations (7) is taken in the form:

$$\bar{W}_c^{(k)}(0,y,s) = A_0^{(k)}\cosh(\lambda_0^{(k)}y) + B_0^{(k)}\sinh(\lambda_0^{(k)}y)$$
$$\bar{W}_c^{(k)}(n,y,s) = A_n^{(k)}\cosh(\lambda_n^{(k)}y) + B_n^{(k)}\sinh(\lambda_n^{(k)}y) \tag{8}$$
$$\bar{\Phi}_c^{*(k)}(0,y,s) = C_0^{(k)} + D_0^{(k)}y,$$
$$\bar{\Phi}_c^{*(k)}(n,y,s) = C_n^{(k)}\cosh(\beta_n y) + D_n^{(k)}\sinh(\beta_n y), \qquad k=1,2 \qquad n=0,1,2,...$$

In Eq. (8), the coefficients A_{nk}, B_{nk}, C_{nk} and D_{nk} $k=1,2$ $n=0,1,2,...$ are unknown. Now, by applying Fourier cosine and Laplace transforms to Eq. (4) and using Eq. (8), In particular, components of the stress and electrical displacement, which are of special interest here may be expressed as:

$$\bar{\sigma}_{zy}^{(k)}(n,y,s) = \gamma^{(k)}\lambda_n^{(k)}[A_{nk}\sinh(\lambda_n^{(k)}y) + B_{nk}\cosh(\lambda_n^{(k)}y)] + e_{15}^{(k)}\beta_n[C_{nk}\sinh(\beta_n y) + D_{nk}\cosh(\beta_n y)], \tag{9}$$

2.1 Dislocation problem

Fundamental solutions for transient problems of two bonded dissimilar piezoelectric materials with finite geometry are derived in a closed form by the distributed dislocation technique in this section. Analogous to the corresponding dislocation problem [21], here it is assumed that bonded rectangular planes are fixed at the edges $y=0,h$ and are traction-free surfaces $x=0,a$. Therefore, the boundary conditions may represented by:

$$\begin{aligned} \sigma_{zx}^{(k)}(m,y,t) = D_x^{(k)}(m,y,t) = 0 \qquad & 0 < y < h,\ m \in \{0,a\}, \\ w^{(k)}(x,m,t) = \varphi^{(k)}(x,m,t) = 0, \qquad & 0 < x < a,\ \ m \in \{0,h\},\ k \in \{1,2\} \end{aligned} \tag{10}$$

The only difficulty in analyzing the crack problems by employing the distributed dislocation technique lies in obtaining the fundamental solution in a medium with a dislocation at the point with arbitrary coordinates. Referring to Fig. (1), a single dynamic electro-elastic dislocation is shown, with a time-dependent Bergers vector $b_{\chi z}$. In the present study, the crack surface is on the electric impermeability conditions. Thus, the electric potential along the dislocation line is multivalued. Along the cut, there are discontinuities in both the mechanical displacement and electric potential:

$$\begin{aligned} w^{(k)}(x,h_2^+,t) - w^{(k)}(x,h_2^-,t) &= b_{\chi z}(t)H(x-\xi), \quad k \in \{1,2\} \\ \varphi^{(k)}(x,h_2^+,t) - \varphi^{(k)}(x,h_2^-,t) &= b_{\chi z}(t)H(x-\xi), \quad ,k \in \{1,2\} \end{aligned} \tag{11}$$

The symbol $H(.)$ is used to denote the Heaviside step function. The continuity conditions required for the shear stress and electric displacement are as follows:

$$\sigma_{zy}^{(1)}(x,h_2^+,t) = \sigma_{zy}^{(2)}(x,h_2^-,t), \qquad D_y^{(1)}(x,h_2^+,t) = D_y^{(2)}(x,h_2^-,t), \tag{12}$$

This section aims to solve Eq. (7) under the conditions (10)–(12), and then to obtain the dynamic fields of stress and electric displacement. Finite Fourier cosine and Laplace transform of Eqs. (10), (11), and (12), lead to the unknown functions, A_{nk}, B_{nk}, C_{nk} and D_{nk}, which are given in Appendix. To avoid dealing with divergent kernels in the numerical calculations, we rewrote the field components into exponential forms. Thus, after performing the routine and lengthy manipulations the expressions for shear stress and electric displacement are then calculated as:

$$\begin{aligned} \bar{\sigma}_{zy}^{(1)}(x,y,s) = & -\frac{\gamma^{(1)}\lambda_0^{(1)}\alpha^{(2)}\zeta b_{wz}(s)}{a(\alpha^{(1)}-\alpha^{(2)})}\frac{\cosh[\lambda_0^{(1)}(y-h)]}{\sinh(\lambda_0^{(1)}h_1)} \\ & + \frac{\gamma^{(1)}b_{wz}(s)}{a}\sum_{n=1}^{\infty}\frac{\lambda_n^{(1)}\Pi_{1n}}{\beta_n}\frac{(1+e^{-2\lambda_n^{(1)}(h-y)})}{(1+e^{-2\lambda_n^{(1)}h})}e^{-\lambda_n^{(1)}(y-h_2)}[\sin(\beta_n(x+\zeta))-\sin(\beta_n(x-\zeta))] \\ & - \frac{e_{15}^{(1)}b_{wz}(s)}{a}\sum_{n=1}^{\infty}\Pi_{2n}\frac{(1+e^{-2\beta_n(h-y)})}{(1+e^{-2\beta_n h})}e^{-\beta_n(y-h_2)}[\sin(\beta_n(x+\zeta))-\sin(\beta_n(x-\zeta))] \\ & + \frac{\gamma^{(1)}\lambda_0^{(1)}\zeta b_{\varphi z}(s)}{a(\alpha^{(1)}-\alpha^{(2)})}\frac{\cosh[\lambda_0^{(1)}(y-h)]}{\sinh(\lambda_0^{(1)}h_1)} \\ & - \frac{\gamma^{(1)}b_{\varphi z}(s)}{a}\sum_{n=1}^{\infty}\frac{\lambda_n^{(1)}\Pi_{3n}}{\beta_n}\frac{(1+e^{-2\lambda_n^{(1)}(h-y)})}{(1+e^{-2\lambda_n^{(1)}h})}e^{-\lambda_n^{(1)}(y-h_2)}[\sin(\beta_n(x+\zeta))-\sin(\beta_n(x-\zeta))] \\ & + \frac{e_{15}^{(1)}b_{\varphi z}(s)}{a}\sum_{n=1}^{\infty}\Pi_{4n}\frac{(1+e^{-2\beta_n(h-y)})}{(1+e^{-2\beta_n h})}e^{-\beta_n(y-h_2)}[\sin(\beta_n(x+\zeta))-\sin(\beta_n(x-\zeta))], \end{aligned}$$

$$\overline{D}_y^{(1)}(x,y,s)=\frac{\varepsilon_{11}^{(1)}b_{wz}(s)}{a}\sum_{n=1}^{\infty}\Pi_{2n}\frac{(1+e^{-2\beta_n(h-y)})}{(1+e^{-2\beta_n h})}e^{-\beta_n(y-h_2)}[\sin(\beta_n(x+\zeta))-\sin(\beta_n(x-\zeta))]$$
$$-\frac{\varepsilon_{11}^{(1)}b_{\varphi z}(s)}{a}\sum_{n=1}^{\infty}\Pi_{4n}\frac{(1+e^{-2\beta_n(h-y)})}{(1+e^{-2\beta_n h})}e^{-\beta_n(y-h_2)}[\sin(\beta_n(x+\zeta))-\sin(\beta_n(x-\zeta))]. \quad (13)$$

where

$$\Pi_{1n}=\frac{\gamma^{(2)}\lambda_n^{(2)}\Theta_{4n}(1+e^{-2\lambda_n^{(2)}h_2})+\alpha^{(2)}\Theta_{2n}(1-e^{-2\lambda_n^{(2)}h_2})}{(\Theta_{1n}\Theta_{4n}-\Theta_{2n}\Theta_{3n})(1-e^{-2\lambda_n^{(2)}h_2})},$$

$$\Pi_{2n}=\frac{\gamma^{(2)}\lambda_n^{(2)}\Theta_{3n}(1+e^{-2\lambda_n^{(2)}h_2})+\alpha^{(2)}\Theta_{1n}(1-e^{-2\lambda_n^{(2)}h_2})}{(\Theta_{1n}\Theta_{4n}-\Theta_{2n}\Theta_{3n})(1-e^{-2\lambda_n^{(2)}h_2})}, \quad (14)$$

$$\Pi_{3n}=\frac{\Theta_{2n}}{\Theta_{1n}\Theta_{4n}-\Theta_{2n}\Theta_{3n}},\Pi_{4n}=\frac{\Theta_{1n}}{\Theta_{1n}\Theta_{4n}-\Theta_{2n}\Theta_{3n}}.$$

The expressions $\Theta_{1n},\Theta_{2n},\Theta_{3n}$ and Θ_{4n} in Eq. (14), are specified in the Appendix. In the numerical examples, the difficulty in obtaining the dynamic stress intensity factors comes from the problematic evaluation of the functions $\Pi_{ln}, l\in\{1,2,3\}$, which are represented by summation that contain singularities.

For further improvement of the numerical calculations, It is necessary to examine the stress and electric displacement components' asymptotic behavior.

2.2 Asymptotic behavior of the field components

The asymptotic behavior of Eq. (13) can be used to obtain the singular behavior of the field components at electro-elastic dislocation. The singularities of the stress and electric displacement may be obtained for large values of the summations variable $n\to\infty$. [18]. Referring now back to (13) and using the following identities for the large value of *n*,

$$\sum_{n=1}^{\infty}e^{-\beta_n(y-h_2)}\sin[\beta_n(x-\zeta)]=\frac{0.5\sin[\frac{\pi}{a}(x-\zeta)]}{\cosh[\frac{\pi}{a}(y-h_2)]-\cos[\frac{\pi}{a}(x-\zeta)]} \quad (15)$$

The field components may be reduced to

$$\overline{\sigma}_{zy}^{(1)}(x,y,s)=-\frac{\gamma^{(1)}\lambda_0^{(1)}\alpha^{(2)}\zeta}{a(\alpha^{(1)}-\alpha^{(2)})}\frac{\cosh[\lambda_0^{(1)}(y-h)]b_{wz}(s)}{\sinh(\lambda_0^{(1)}h_1)}+\frac{\gamma^{(1)}b_{wz}(s)}{a}$$
$$\times\sum_{n=1}^{\infty}[\frac{\lambda_n^{(1)}\Pi_{1n}}{\beta_n}\frac{(1+e^{-2\lambda_n^{(1)}(h-y)})}{(1+e^{-2\lambda_n^{(1)}h})}e^{-\lambda_n^{(1)}(y-h_2)}-\Pi_{1\infty}e^{-\beta_n(y-h_2)}]$$
$$\times[\sin(\beta_n(x+\zeta))-\sin(\beta_n(x-\zeta))]$$
$$-\frac{e_{15}^{(1)}b_{wz}(s)}{a}\sum_{n=1}^{\infty}[\Pi_{2n}\frac{(1+e^{-2\beta_n(h-y)})}{(1+e^{-2\beta_n h})}e^{-\beta_n(y-h_2)}-\Pi_{2\infty}e^{-\beta_n(y-h_2)}]$$
$$\times[\sin(\beta_n(x+\zeta))-\sin(\beta_n(x-\zeta))]$$
$$+\frac{\gamma^{(1)}\lambda_0^{(1)}\zeta}{a(\alpha^{(1)}-\alpha^{(2)})}\frac{\cosh[\lambda_0^{(1)}(y-h)]b_{\varphi z}(s)}{\sinh(\lambda_0^{(1)}h_1)}-\frac{\gamma^{(1)}b_{\varphi z}(s)}{a}$$
$$\times\sum_{n=1}^{\infty}[\frac{\lambda_n^{(1)}\Pi_{3n}}{\beta_n}\frac{(1+e^{-2\lambda_n^{(1)}(h-y)})}{(1+e^{-2\lambda_n^{(1)}h})}e^{-\lambda_n^{(1)}(y-h_2)}-\Pi_{3\infty}e^{-\beta_n(y-h_2)}]$$
$$\times[\sin(\beta_n(x+\zeta))-\sin(\beta_n(x-\zeta))]$$
$$+\frac{e_{15}^{(1)}b_{\varphi z}(s)}{a}\sum_{n=1}^{\infty}[\Pi_{4n}\frac{(1+e^{-2\beta_n(h-y)})}{(1+e^{-2\beta_n h})}e^{-\beta_n(y-h_2)}-e^{-\beta_n(y-h_2)}\Pi_{4\infty}]$$
$$\times[\sin(\beta_n(x+\zeta))-\sin(\beta_n(x-\zeta))]$$
$$+\frac{(\gamma^{(1)}\Pi_{1\infty}-e_{15}^{(1)}\Pi_{2\infty})b_{wz}(s)}{2a}[S(x+\zeta,y-h_2)-S(x-\zeta,y-h_2)]$$
$$-\frac{(\gamma^{(1)}\Pi_{3\infty}-e_{15}^{(1)}\Pi_{4\infty})b_{\varphi z}(s)}{2a}[S(x+\zeta,y-h_2)-S(x-\zeta,y-h_2)],\quad(16)$$

$$\overline{D}_y^{(1)}(x,y,s)=\frac{\varepsilon_{11}^{(1)}b_{wz}(s)}{a}\sum_{n=1}^{\infty}[\Pi_{2n}\frac{1+e^{-2\beta_n(h-y)}}{1+e^{-2\beta_n h}}e^{-\beta_n(y-h_2)}-\Pi_{2\infty}e^{-\beta_n(y-h_2)}]$$
$$\times[\sin(\beta_n(x+\zeta))-\sin(\beta_n(x-\zeta))]$$
$$-\frac{\varepsilon_{11}^{(1)}b_{\varphi z}(s)}{a}\sum_{n=1}^{\infty}[\Pi_{4n}\frac{1+e^{-2\beta_n(h-y)}}{1+e^{-2\beta_n h}}e^{-\beta_n(y-h_2)}-\Pi_{4\infty}e^{-\beta_n(y-h_2)}]$$
$$\times[\sin(\beta_n(x+\zeta))-\sin(\beta_n(x-\zeta))]$$
$$+\frac{\varepsilon_{11}^{(1)}\Pi_{2\infty}b_{wz}(s)}{2a}[S(x+\zeta,y-h_2)-S(x-\zeta,y-h_2)]$$
$$-\frac{\varepsilon_{11}^{(1)}\Pi_{4\infty}b_{\varphi z}(s)}{2a}[S(x+\zeta,y-h_2)-S(x-\zeta,y-h_2)],$$

where

$$S(q_1,q_2)=\frac{\sin(\pi q_1/a)}{\cosh(\pi q_2/a)-\cos(\pi q_1/a)} \tag{17}$$

and

$$\Pi_{1\infty}=\frac{\gamma^{(2)}(1+\frac{\varepsilon_{11}^{(1)}}{\varepsilon_{11}^{(2)}})+\alpha^{(2)}(e_{15}^{(1)}-e_{15}^{(2)}\frac{\varepsilon_{11}^{(1)}}{\varepsilon_{11}^{(2)}})}{(\gamma^{(1)}+\gamma^{(2)})(1+\frac{\varepsilon_{11}^{(1)}}{\varepsilon_{11}^{(2)}})-(e_{15}^{(1)}-e_{15}^{(2)}\frac{\varepsilon_{11}^{(1)}}{\varepsilon_{11}^{(2)}})(\alpha^{(1)}-\alpha^{(2)})},$$

$$\Pi_{2\infty}=\frac{\gamma^{(2)}(\alpha^{(1)}-\alpha^{(2)})+\alpha^{(2)}(\gamma^{(1)}+\gamma^{(2)})}{(\gamma^{(1)}+\gamma^{(2)})(1+\frac{\varepsilon_{11}^{(1)}}{\varepsilon_{11}^{(2)}})-(e_{15}^{(1)}-e_{15}^{(2)}\frac{\varepsilon_{11}^{(1)}}{\varepsilon_{11}^{(2)}})(\alpha^{(1)}-\alpha^{(2)})},$$

$$\Pi_{3\infty}=\frac{(e_{15}^{(1)}-e_{15}^{(2)}\frac{\varepsilon_{11}^{(1)}}{\varepsilon_{11}^{(2)}})}{(\gamma^{(1)}+\gamma^{(2)})(1+\frac{\varepsilon_{11}^{(1)}}{\varepsilon_{11}^{(2)}})-(e_{15}^{(1)}-e_{15}^{(2)}\frac{\varepsilon_{11}^{(1)}}{\varepsilon_{11}^{(2)}})(\alpha^{(1)}-\alpha^{(2)})}, \tag{18}$$

$$\Pi_{4\infty}=\frac{\gamma^{(1)}+\gamma^{(2)}}{(\gamma^{(1)}+\gamma^{(2)})(1+\frac{\varepsilon_{11}^{(1)}}{\varepsilon_{11}^{(2)}})-(e_{15}^{(1)}-e_{15}^{(2)}\frac{\varepsilon_{11}^{(1)}}{\varepsilon_{11}^{(2)}})(\alpha^{(1)}-\alpha^{(2)})}$$

We find that, Eqs. (16) have Cauchy-type singularities as $x\to\xi$, $y\to h_2$. The validity of this claim has been discussed in [18] and [21].

2.3 Interfacial cracks formulation

In the analysis given here, the disturbance in the field components due to a single and two interacting interfacial cracks is considered. However, the proposed method in this investigation can be extended to analyze more than two interacting cracks lying on the interface of bonded piezoelectric rectangular planes. Therefore, we employ a general strategy to construct the singular integral equations by distributing the dislocations with unknown density $B_{wzj}(r,s)$ and $B_{\phi j}(r,s)$ for N interacting interfacial cracks [22]. Furthermore, the geometry of the interfacial crack can be represented parametrically as follows:

$$x_i(p) = x_{ic} + L_i p\,,$$
$$y_i(p) = h_2 \qquad i \in \{1,2,...,N_1\},\ -1 \le p \le 1 \tag{19}$$

the crack center coordinates are denoted by (x_{ic}, h_2). The following singular integral equations, express the requirement of the traction-free and charge-free conditions on the crack surfaces:

$$\tilde{\sigma}_{zy}(x_i, y_i, s) = \sum_{j=1}^{N} L_j \int_{-1}^{+1} [K_{ij11}(p,r,s) B_{wzj}(r,s) + K_{ij12}(p,r,s) B_{\varphi j}(r,s)]dr,$$
$$\tilde{D}_y(x_i, y_i, s) = \sum_{j=1}^{N} L_j \int_{-1}^{+1} [K_{ij21}(p,r,s) B_{wzj}(r,s) + K_{ij22}(p,r,s) B_{\varphi j}(r,s)]dr \tag{20}$$

The kernels contain Cauchy terms, and the dislocation densities on the crack border are unknown functions. These functions are determined by imposing the following single-valuedness conditions

$$\int_{-1}^{1} B_{kj}(r,s)dr = 0, \qquad k \in \{wz, \varphi\},\ -1 \le r \le 1,\ \ j \in \{1,2,...,N\} \tag{21}$$

By considering the dominant part of the integral equations (20), the appropriate representation of the dislocation density is [23]:

$$B_{kj}(r,s) = \frac{g_{kj}(r,s)}{\sqrt{1-r^2}}, \qquad k \in \{wz, \varphi\}, \qquad j \in \{1,2,...,N\} \tag{22}$$

The bonded functions $g_{ki}(r,s)$ are obtained by using the numerical method described in [23]. Then, the dynamic stress and electric displacement intensity factors at the crack tips are defined by [8].

$$K_{MRi}(\mathrm{s}) = -\frac{\sqrt{L(1)}}{2}[c_{44} g_{zi}(1,s) + e_{15} g_{\varphi i}(1,s)]\,,$$
$$K_{MLi}(\mathrm{s}) = \frac{\sqrt{L(-1)}}{2}[c_{44} g_{zi}(-1,s) + e_{15} g_{\varphi i}(-1,s)]\,,$$
$$K_{DRi}(\mathrm{s}) = -\frac{\sqrt{L(1)}}{2}[e_{15} g_{zi}(1,s) - d_{11} g_{\varphi i}(1,s)],$$
$$K_{DLi}(\mathrm{s}) = \frac{\sqrt{L(-1)}}{2}[e_{15} g_{zi}(-1,s) - d_{11} g_{\varphi i}(-1,s)]. \tag{23}$$

The subscripts R and L stand for the right and left tips of each crack, respectively. By applying the inverse of the Laplace transform to Eq. (23), the dynamic stress intensity factors (DSIFs) are determined. The inverse Laplace transforms of DSIFs are obtained by using Stehfest's method [24].

3 Results and discussion

The interfacial crack formulation described in the previous sections can be applied to bonded dissimilar rectangular piezoelectric planes containing any number of cracks with ease. The elastic problem of a cracked isotropic rectangular plane has been considered before by Faal and Dehghan [18]. The verification of analysis is performed by considering the above-mentioned paper with no piezoelectric effect, by setting $c_{44}^{(1)} = c_{44}^{(1)}, e_{15}^{(1)} = e_{15}^{(2)} = 0$ and $\varepsilon_{11}^{(1)} = \varepsilon_{11}^{(2)} = 0$, the stress components (13) reduced to

$$\sigma_{zy}(x,y) = \frac{2b_{wz}c_{44}}{a}\sum_{n=1}^{\infty}\frac{\sin(\beta_n\xi)\cosh(\beta_n h_2)}{\sinh(\beta_n h)}\cosh[\beta_n(h-y)]\cos(\beta_n x) \qquad 0 < y < h_2$$
$$\sigma_{zy}(x,y) = \frac{2b_{wz}c_{44}}{a}\sum_{n=1}^{\infty}\frac{\sin(\beta_n\xi)\cosh(\beta_n h_1)}{\sinh(\beta_n h)}\cosh(\beta_n y)\cos(\beta_n x) \qquad h_2 < y < h \tag{24}$$

First, some numerical calculations are carried out to compare the results with those given in open literature. Hence, some verifications were performed with the results of Faal and Dehghan [18]. Table 1 shows the results of the stress intensity factor at the horizontal crack tip in an isotropic elastic plane subjected to the out-of-plane shear traction on its surfaces. The comparisons of SIFs versus the non-dimensional crack location and length are carried out. The stress intensity factors are compared to those reported by Faal and Dehghan [18]. Which are in excellent agreement with the present work.

Table (2) displays the dynamic stress intensity factors for a crack in an elastic rectangular plane subjected to an out-of-plane impact load. The results are reasonably consistent with those presented by Zhang and Ma. [25]. In this paper, some additional results are given and the electromechanical uniform impact loadings $\sigma_{zy} = \tau_0 H(t)$ and $D_y = D_0 H(t)$ are applied at crack faces. Furthermore, to reflect the effects of compound mechanical and electrical impacts, the electromechanical coupling ratio is defined by [8].

$$\lambda_D = D_0 e_{150} / \tau_0 \varepsilon_{110} \tag{25}$$

In the numerical results, the loading parameters are chosen as $\lambda_D = 1.0$ and dimensionless plane dimensions are $a/h = 1.0$ and $h_1/h = h_2/h = 0.5$.

Table 1 Stress intensity factors for an isotropic plane $a = h$.

y_c/h		$2L/h = 0.1$	$2L/h = 0.2$	$2L/h = 0.3$	$2L/h = 0.4$
0.95	Current Study	1.098	1.286	1.541	1.916
	Faal and Dehgan [18]	1.097	1.284	1.531	1.913
0.9	Current Study	1.035	1.131	1.274	1.488
	Faal and Dehgan [18]	1.033	1.128	1.272	1.487
0.75	Current Study	1.010	1.059	1.136	1.268
	Faal and Dehgan [18]	1.011	1.059	1.136	1.269
0.5	Current Study	1.007	1.049	1.123	1.243
	Faal and Dehgan [18]	1.009	1.048	1.120	1.242

Table 2 Non-dimensional DSIFs at the crack tip in an elastic square plane

$2L:a:h$		$c_s t/L=1$	$c_s t/L=2$	$c_s t/L=3$	$c_s t/L=4$	$c_s t/L=5$
1:10:10	Current Study Zhang and Ma [25]	0.9042 0.8978	1.225 1.2472	1.1301 1.1281	1.0318 1.0297	1.0060 1.0056
2:10:10	Current Study Zhang and Ma [25]	0.8976 0.8999	1.2348 1.2498	1.1304 1.1257	1.0295 1.0392	0.9991 1.0204
3:10:10	Current Study Zhang and Ma [25]	0.8995 0.9022	1.2560 1.2664	1.1211 1.1290	1.0282 1.0582	1.0591 1.0432
4:10:10	Current Study Zhang and Ma [25]	0.8995 0.9024	1.2415 1.2519	1.1289 1.1386	1.0654 1.0878	1.0899 1.0787
5:10:10	Current Study Zhang and Ma [25]	0.8965 0.8943	1.221 1.2308	1.1916 1.1800	1.1460 1.1472	1.01501 1.01390

Table 3 Material constants [26].

Piezoelectric material	**Elastic stiffness** $c_{44}(10^{10}\,N/m^2)$	**Piezoelectric constant** $e_{15}(C/m^2)$	**Dielectric constant** $\varepsilon_{11}(10^{-10}\,C/Vm)$	**Mass density** $\rho(10^3\,kg/m^3)$
PZT-4	2.56	13.44	60	7.5
PZT-5H	2.30	17.44	150.3	7.6
PZT-6B	2.71	4.6	36	7.55
PZT-7A	2.54	9.7	81.1	7.5

In addition, piezoelectric materials used in the numerical calculations are listed in Table (3). In the proceeding example, time is normalized by $t_0 = L/c_s$, and the DSIFs and electric displacement factor are normalized by $K_0 = \tau_0\sqrt{L}$ and $K_{0D} = D_0\sqrt{L}$, respectively. It is clear that, the field intensity factors are dependent on the convergence of the series which is very sensitive to the ratios L/h and h_1/h_2. To reach at a certain accuracy, the number of terms are required in the series is $n = 280$.

Fig. (2a) shows the geometry of the bonded piezoelectric rectangular plane with an interface crack. The results of single crack problems are shown in Figs. (2b-2e). Here referring to Fig. (2b), variations of the dimensionless dynamic stress intensity factors (DSIFs) of an interface crack as a function of the normalized time, t/t_0 for three different material combinations are presented.

Generally speaking, by increasing the normalized time, the value of the DSIFs rises rapidly to reach a peak value and then goes to a steady state value. Furthermore, it is seen that DSIFs in the layered composite with PZT-4 and PZT-6B arrangement of material are the largest. Similar results are shown in Fig. (2c) for the variations of the electric displacement factor.

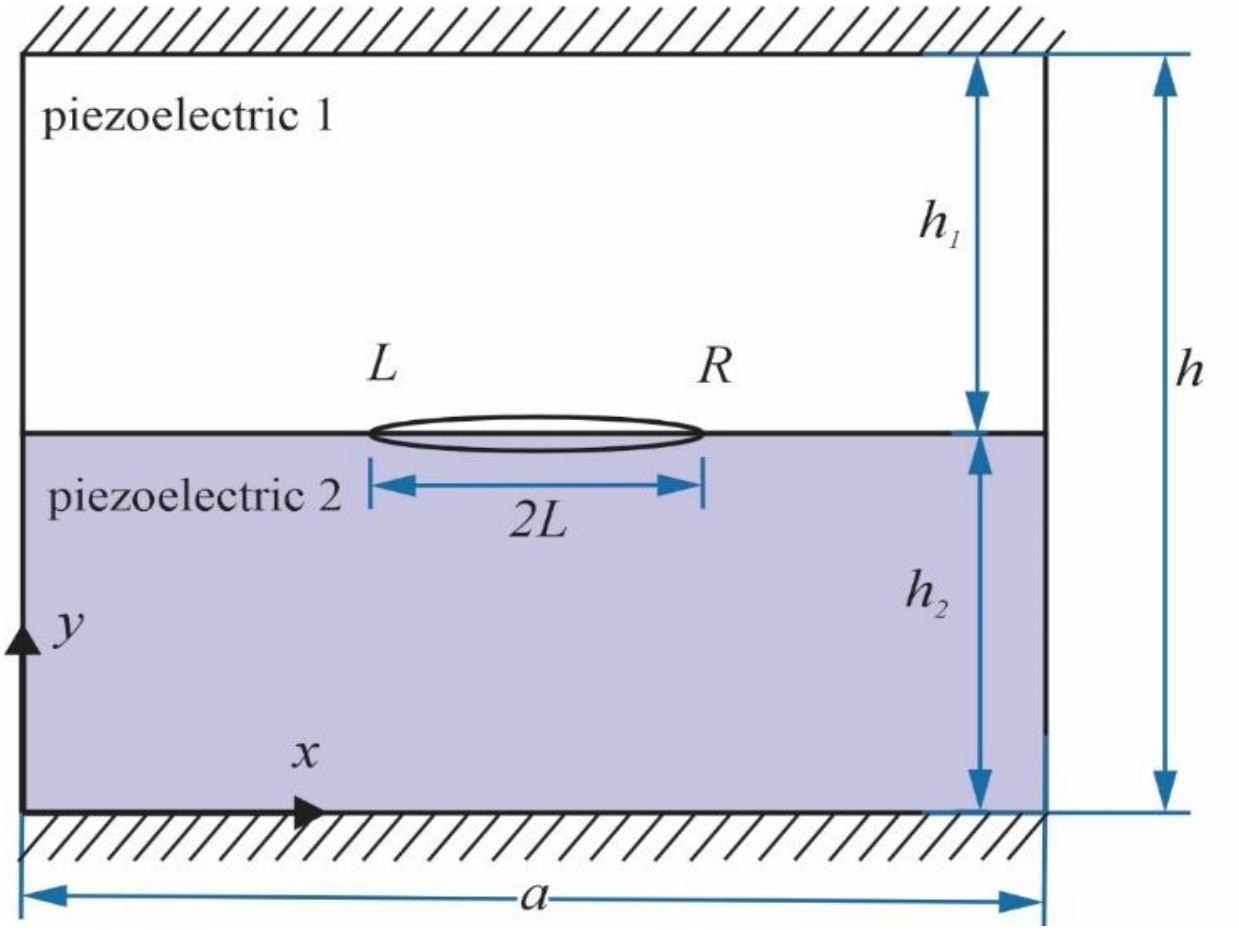

Figure 2(a) Bonded dissimilar piezoelectric rectangular plane with an interface crack

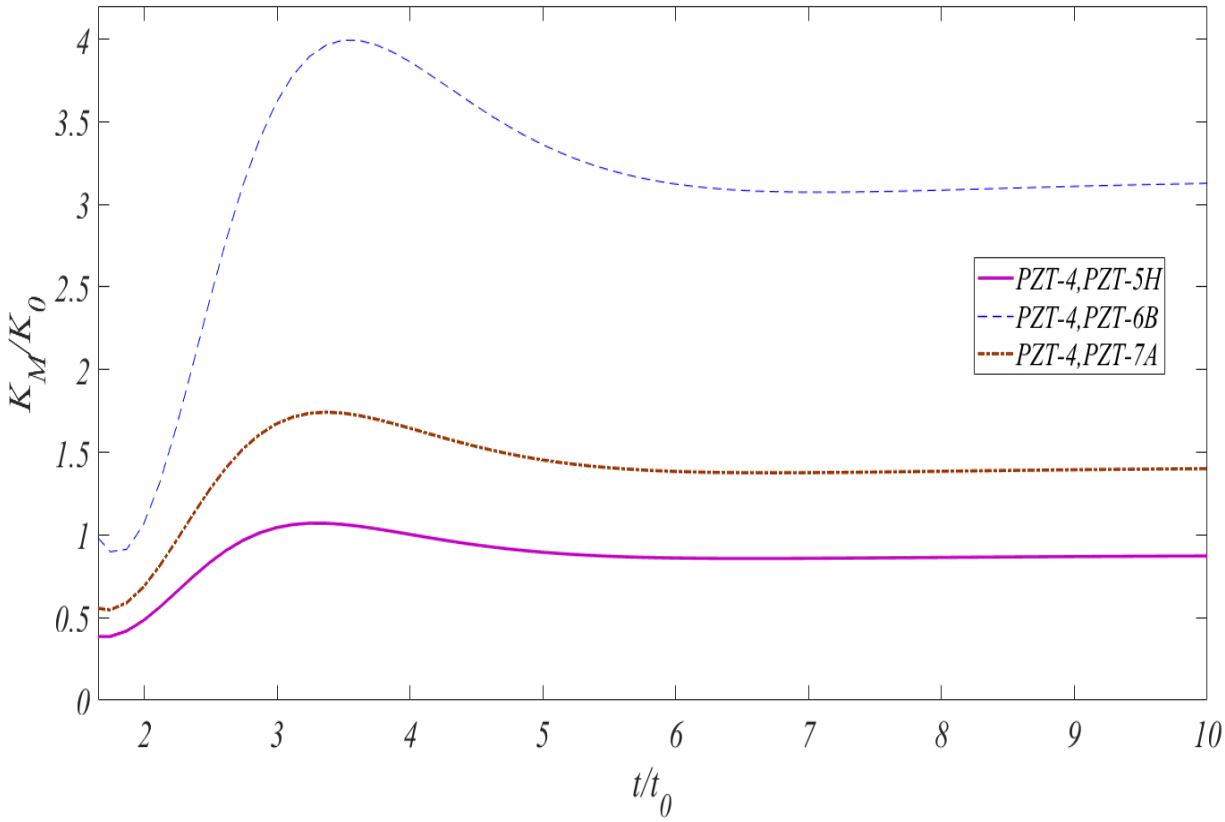

Figure 2(b) Dynamic stress intensity factors for different piezoelectric materials of the lower

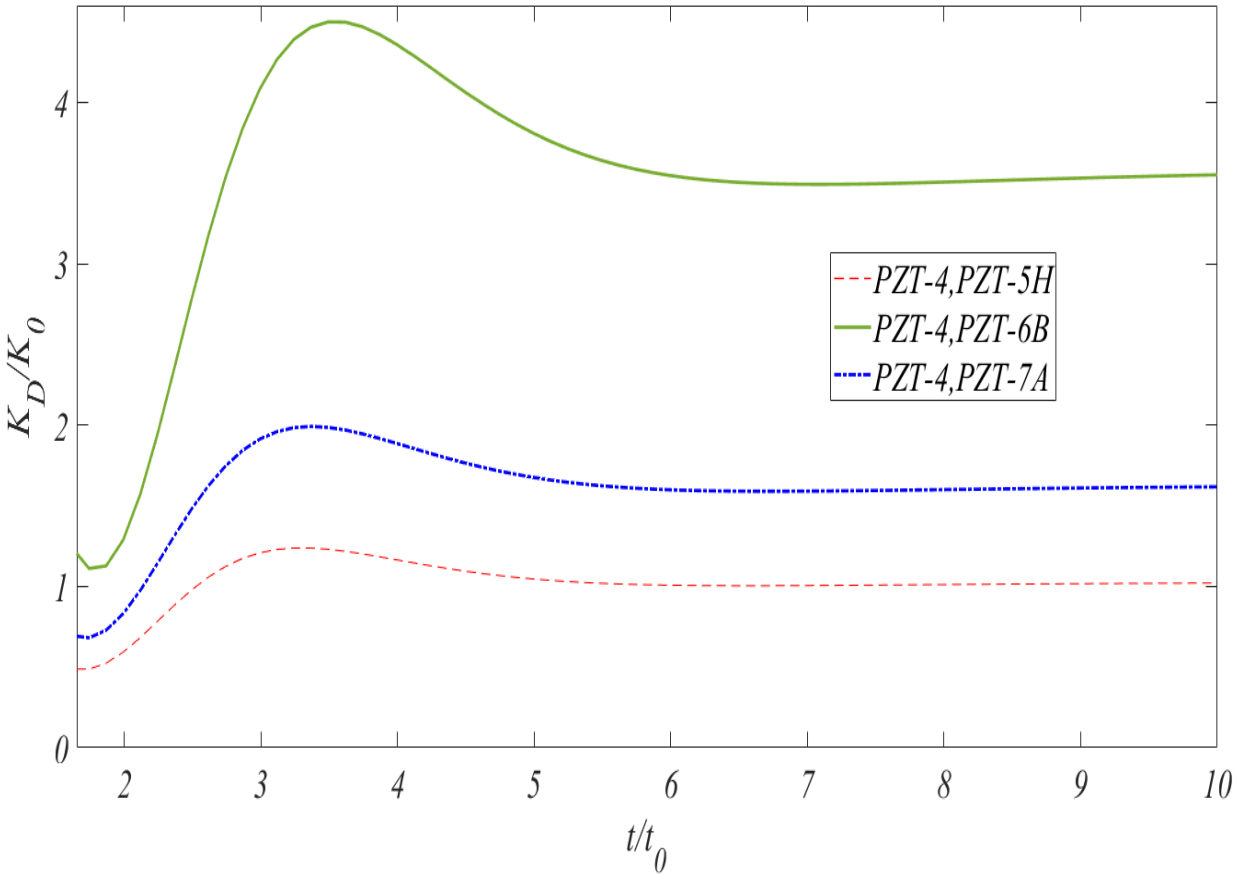

Figure 2(c) Electric displacement stress intensity factors for different piezoelectric materials of the lower layer

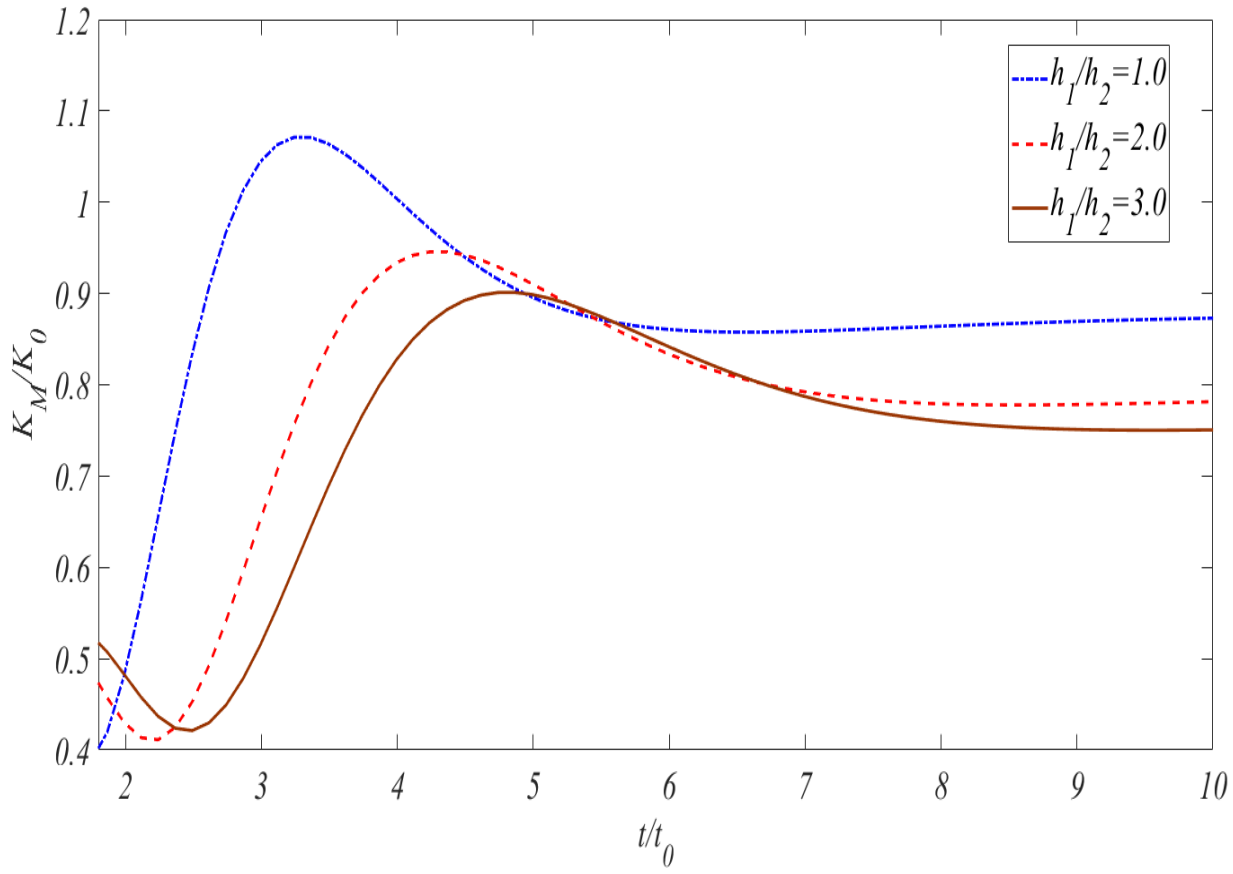

Figure 2(d) Normalized stress intensity factors for different ratio of plane thicknesses

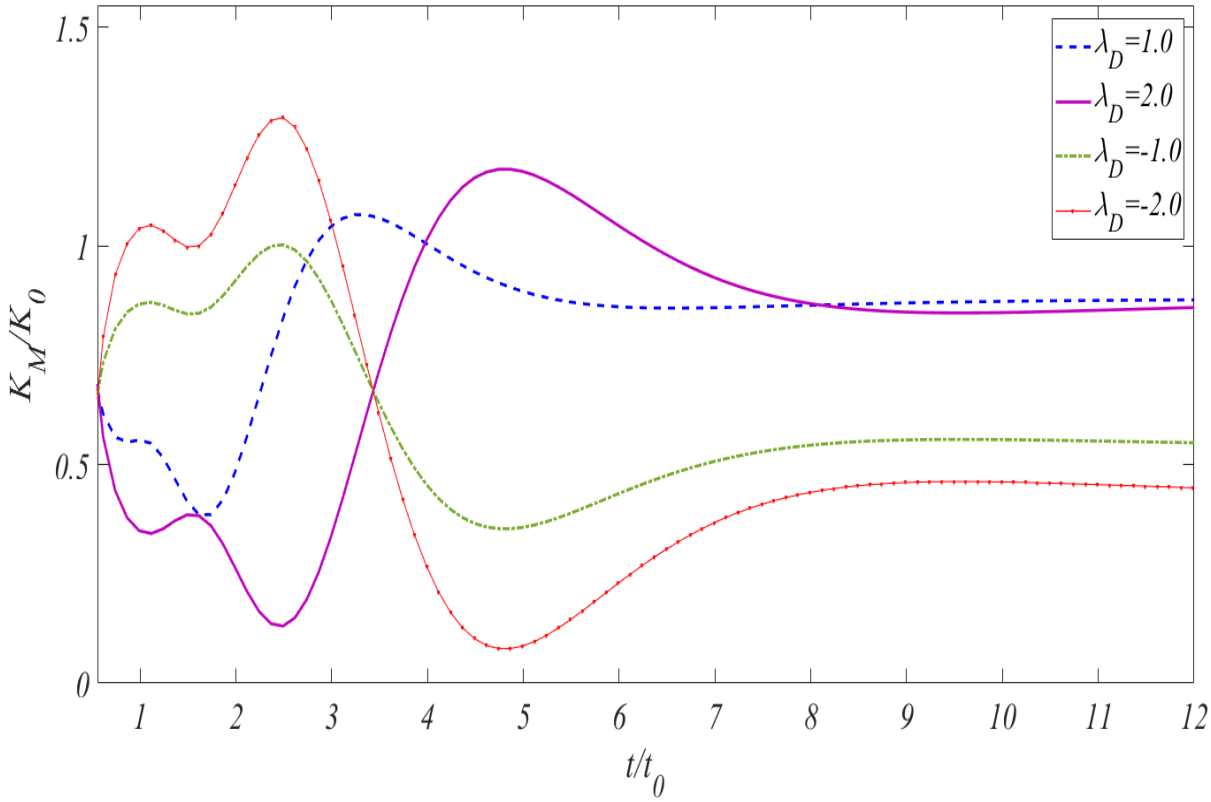

Figure 2(e) Normalized stress intensity factors for different values of electromechanical coupling factors

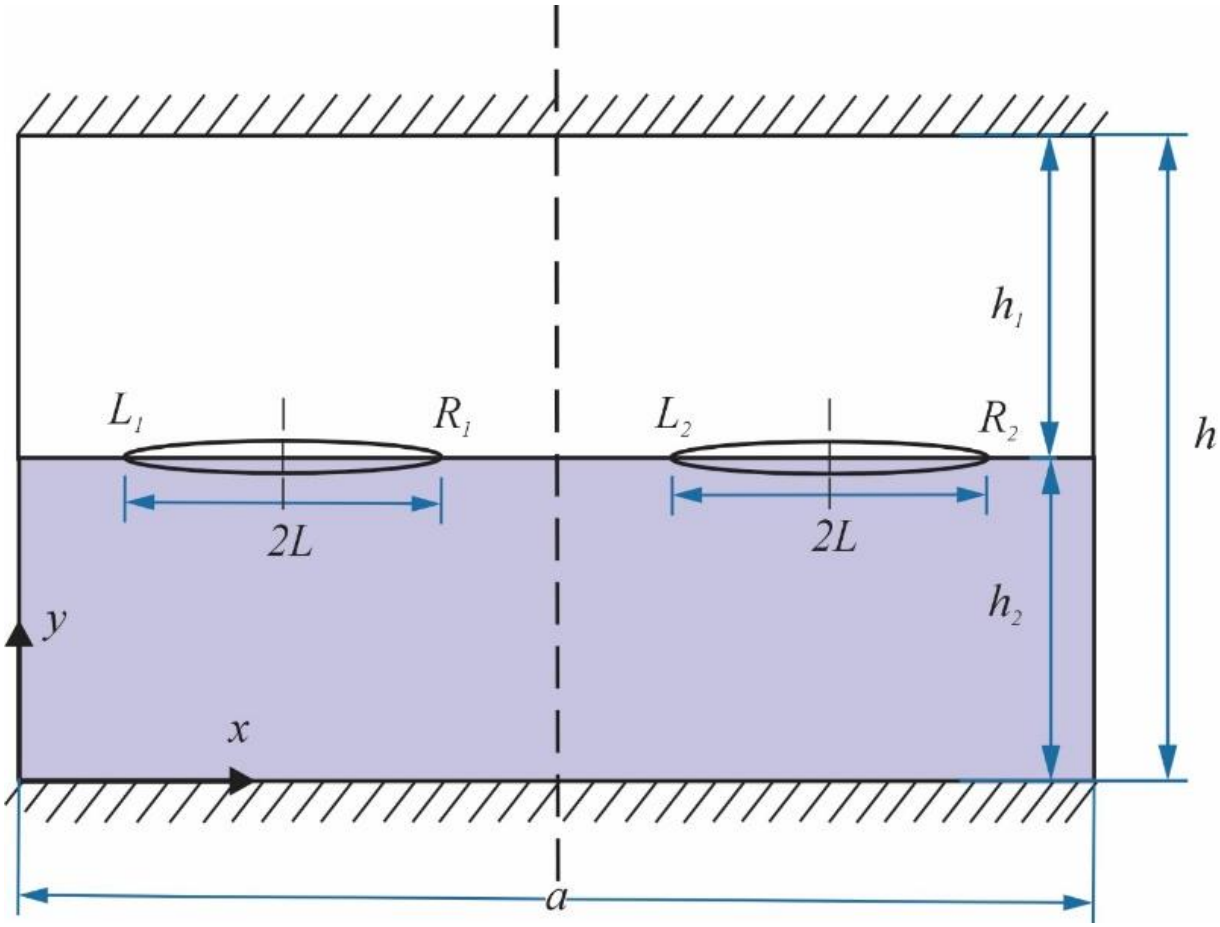

Figure 3(a) Bonded dissimilar piezoelectric rectangular plane with two equal-length interfacial crack

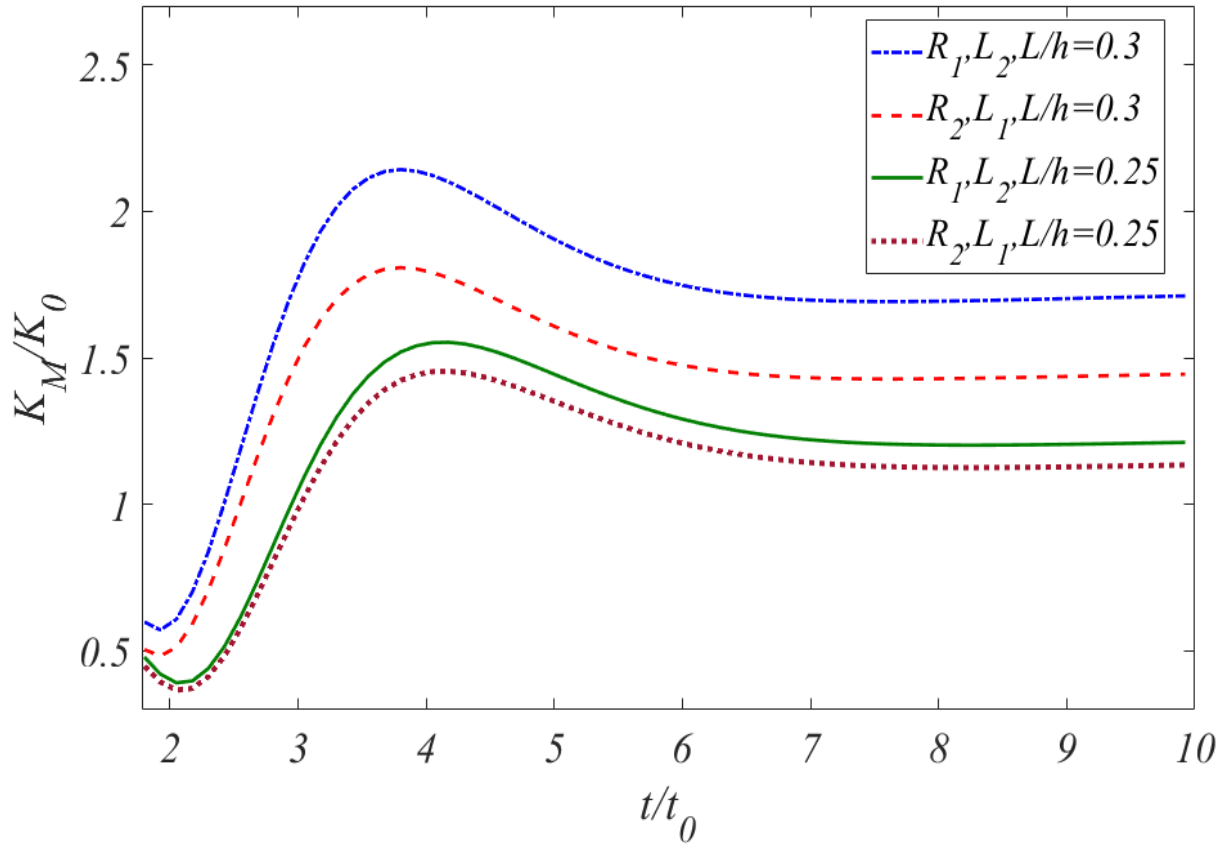

Figure 3(b) Dynamic stress intensity factors of two interfacial cracks versus crack length

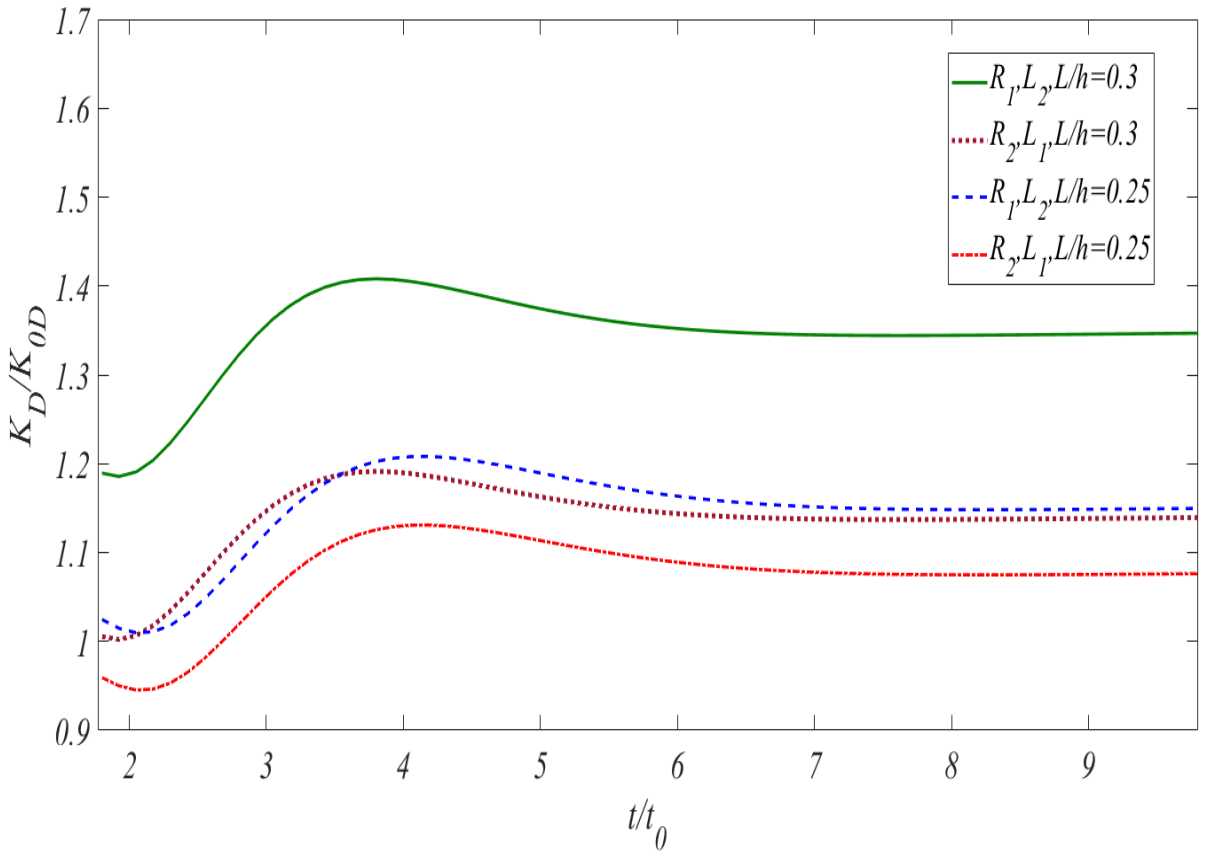

Figure 3(c) Electric displacement factors of two interfacial cracks versus crack length

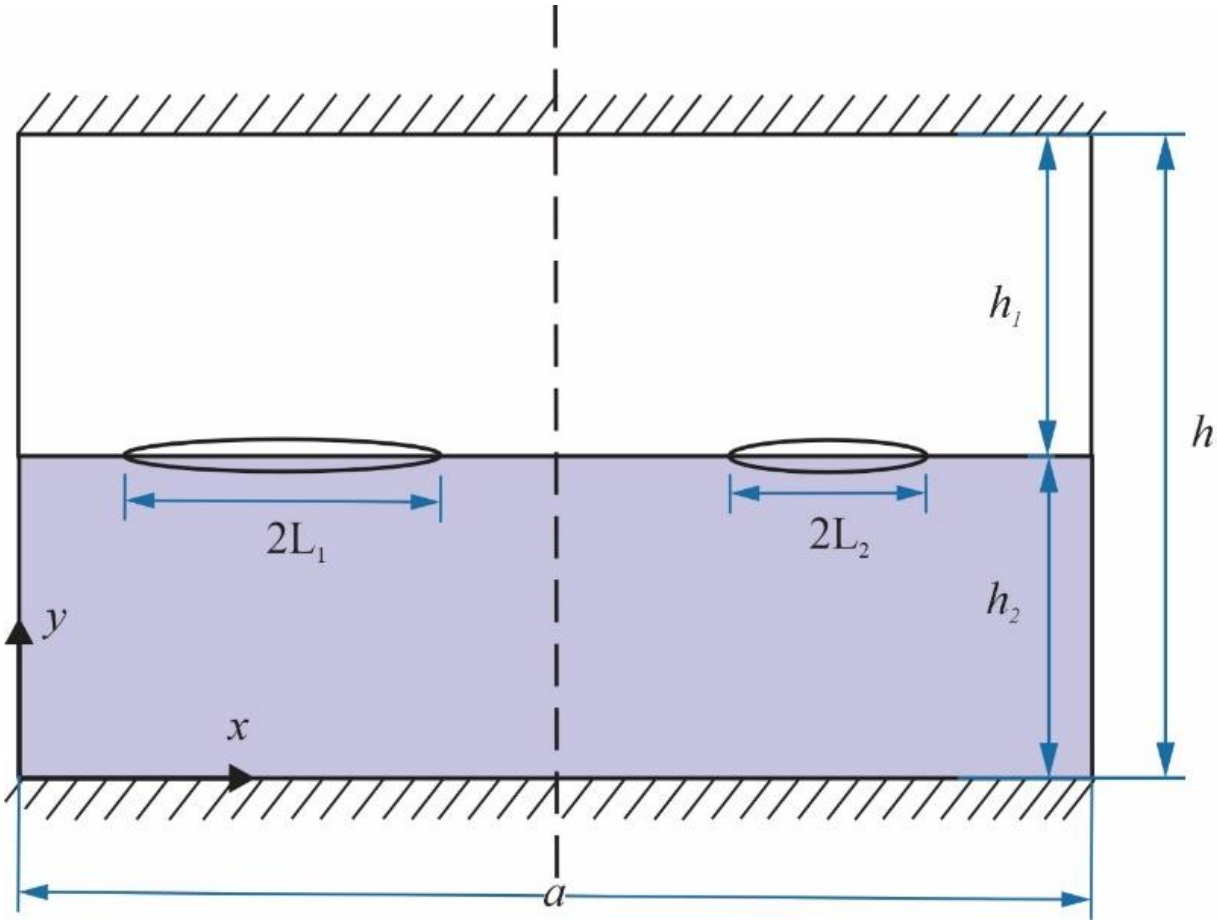

Figure 4(a) Bonded dissimilar piezoelectric rectangular plane with two interacting interfacial cracks

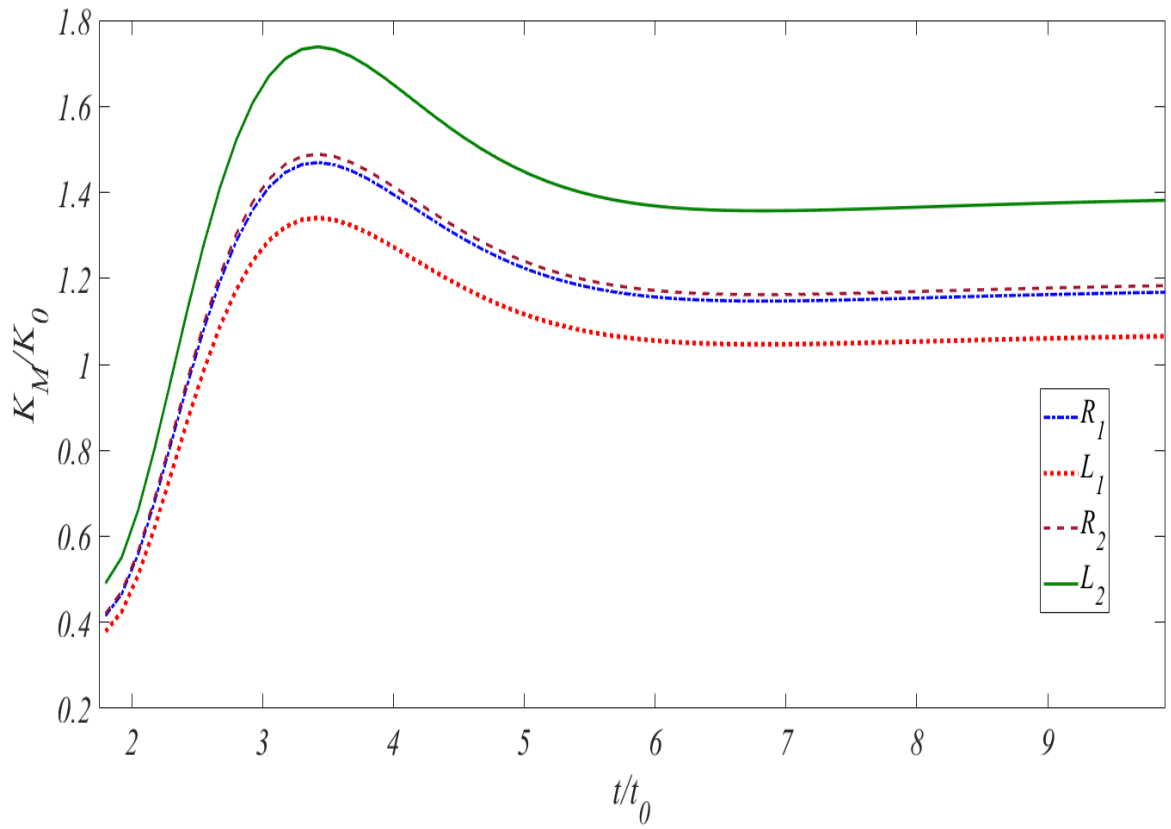

Figure 4(b) Dynamic stress intensity factors of two interacting interfacial cracks

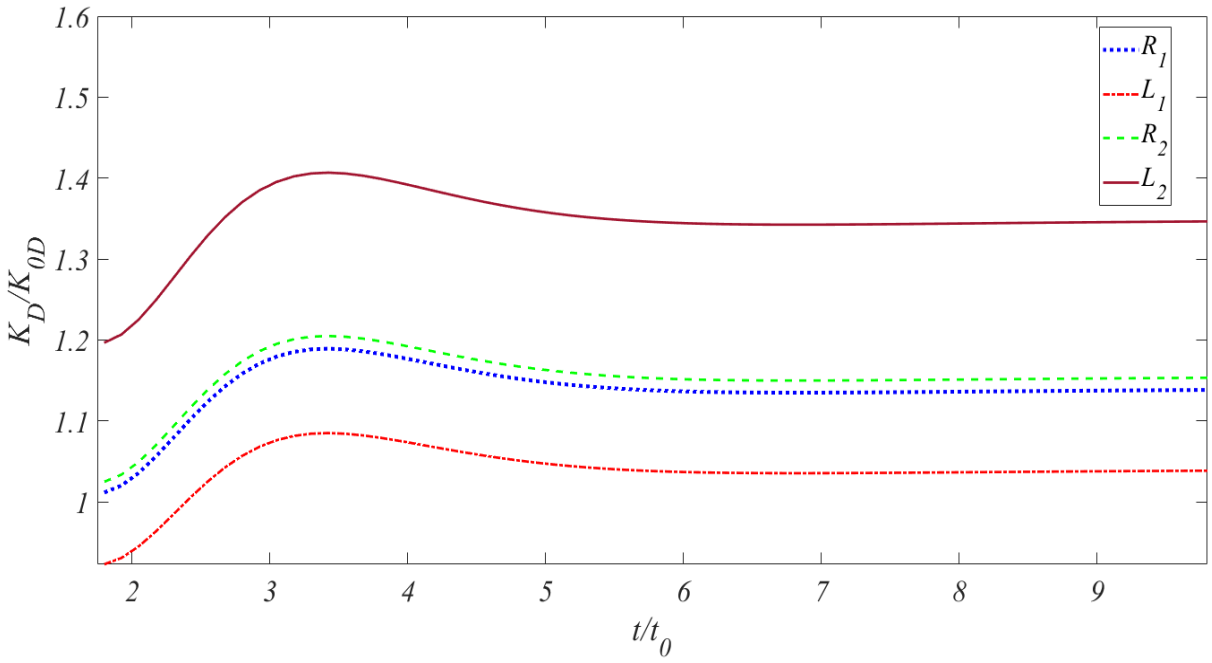

Figure 4(c) Electric displacement factors of two interacting interfacial cracks.

To study the influence of rectangular plane thickness on DSIF, an interface crack in bonded dissimilar piezoelectric planes under uniform electromechanical impact loadings, is considered, Fig. (2d). It can be found that, in all materials, as the h_1/h_2 increases, the peak value of DSIFs diminishes, It is a fact that DSIF takes a significantly longer time to reach its maximum value. The next example examines the effect of the loading parameter λ_D on DSIFs (Fig. 2e).

It is observed that the positive and negative loading factors at different stages of loading may intensify or delay the process of crack initiation at the interface. It has been observed that the DSIFs undergo significant changes depending on the sign of the loading parameter.The times at which the maximum of DSIFs occur for small values of positive loading parameter are shorter than larger values whereas, it does not have a remarkable difference for a negative sign of loading parameter and the normalized dynamic DSIF approaches the static value in an oscillating way. The interaction between two equal-length interfacial cracks is studied in the next example (Fig. 3a).

The problem has a symmetry; hence only the variations of DSIFs of the right tip of the left crack were considered. Fig. (3b) shows the effect of crack length on DSIFs. As expected, larger cracks resulted in higher DSIFs. The maximum values of DSIFs at the tip of the interface crack with different lengths, do not occur simultaneously. For the smaller crack, It takes a significantly longer time for DSIF to attain its static value. Note that the peaks are more pronounced if the crack length is increased. Similar to the DSIFs, as the crack length increases, the electric displacement factor (EDFs) at the crack tips increases and then the peak value of dynamic EDF increases notably.

This formulation can be used to analyze the problem of several asymmetric interfacial cracks. (Fig. 4a).

The dynamic stress intensity factors (DSIFs) experience a sudden increase from negative values to a peak value that is higher than its static value. After reaching the static value, the DSIFs then oscillate around it. The crack length was first selected to be $L_1/h = 0.3$ and next to be $L_1/h = 0.15$. In Fig. (4c) the variations of Electric displacement factors (EDFs) are plotted against non-dimensional time for selected values of crack length $L_1/h = 0.3$ and $L_1/h = 0.15$. As the length of the cracks decreases, the interaction of cracks attenuates.

4 Conclusions

The dynamic behavior of the cracked bonded dissimilar piezoelectric planes has been analyzed theoretically by using the integral transforms method. Discussions were held on the interaction of multiple interfacial cracks in a bonded piezoelectric medium under uniform electro-mechanical impacts using the distributed dislocation technique. The following conclusions can be made from the numerical results:

- The crack initiation can be enhanced or retarded depending on the electromechanical loading.
- The crack growth could be either enhanced or retarded by the arrangement of piezoelectric material in the layered composite.
- The thickness of the rectangular planes can significantly affect the fracture behavior of the cracked layered composites.
- The dynamic crack propagation is enhanced by a large absolute value of the electromechanical coupling factor, while small values retard the dynamic crack growth.
- The overshoot of dynamic stress intensity factors is significantly amplified or reduced depending on sign of electromechanical loading parameter.
- Results indicated that the inner crack tip is more prone to propagate under dynamic loadings than the outer crack tip. Additionally, the closer the distance between two cracks, the easier the crack growth.

References

[1] A. K. Soh, D. N. Fang, and K. L. Lee, "Analysis of a Bi-piezoelectric Ceramic Layer with an Interfacial Crack Subjected to Anti-plane Shear and In-plane Electric Loading", *European Journal of Mechanics-A/Solids*, Vol. 19, pp. 961–977, 2000, https://doi.org/10.1016/S0997-7538(00)01107-4.

[2] B. Gu, X. Wang, S. Yu, and D. Gross, "Transient Response of a Griffith Crack between Dissimilar Piezoelectric Layers under Anti-plane Mechanical and In-plane Electrical Impacts", *Engineering Fracture Mechanics*, Vol. 69, pp. 565–576, 2002, https://doi.org/10.1016/S0013-7944(01)00100-X.

[3] X. Zhao, S. A. Meguid, and K. M. Liew, "The Transient Response of Bonded Piezoelectric and Elastic Half-space with Multiple Interfacial Collinear Cracks", *Acta Mechanica*, Vol. 159, pp. 11–27, 2002, https://doi.org/10.1007/BF01171444.

[4] W. J. Feng, Z. W. Zou, R. K. L. Su, and Z. Z. Zou, "Dynamic Response of Multiple Coplanar Interface Cracks between Two Dissimilar Piezoelectric Materials", *Key Engineering Materials*, Vols. 261-263, pp. 477–482, 2004, https://doi.org/10.4028.

[5] Z. T. Chen, "Interfacial Coplanar Cracks in Piezoelectric Bi-material Systems under Pure Mechanical Impact Loading", *International Journal of Solids and Structures*, Vol. 43, pp. 5085–5099, 2006, https://doi.org/10.1016/j.ijsolstr.2005.07.017.

[6] Y. S. Ing, and J. H. Chen, "Dynamic Fracture Analysis of an Interfacial Crack in a Two-layered Functionally Graded Piezoelectric Strip", *Theoretical and Applied Fracture Mechanics*, Vols. 63-64, pp. 40–49, 2013, https://doi.org/10.1016/j.tafmec.2013.03.004.

[7] J. W. Shin, and T. U. Kim, "Transient Response of a Mode III Interface Crack between the Piezoelectric Layer and Functionally Graded Orthotropic Layer", *International Journal of Solids and Structures*, Vol. 90, pp. 122–128, 2016, https://doi.org/10.1016/j.ijsolstr.2016.03.033.

[8] A. H. Fartash, M. Ayatollahi, and R. Bagheri, "Transient Response of Dissimilar Piezoelectric Layers with Multiple Interacting Interface Cracks", *Applied Mathematical Modelling*, Vol. 66, pp. 508–526, 2019, https://doi.org/10.1016/j.apm.2018.09.030.

[9] S. S. Chang, "The Solution of a Rectangular Orthotropic Sheet with a Central Crack under Anti-plane Shear", *Engineering Fracture Mechanics*, Vol. 22, pp. 253–261, 1985, https://doi.org/10.1016/S0013-7944(85)80027-8.

[10] S. W. Ma, "A Central Crack of Mode III in a Rectangular Sheet with Fixed Edges", *International Journal of Fracture*, Vol. 39, pp. 323–329, 1989, https://doi.org/10.1007/BF00017704.

[11] X. S. Zhang, "A Finite Rectangular Sheet with a Pair of Edge Cracks Excited by a Normal Anti-plane Shear Wave", *Engineering Fracture Mechanics*, Vol. 35, pp. 1037–1042, 1990, https://doi.org/10.1016/0013-7944(90)90131-Y.

[12] S. W. Ma, and L. X. Zhang, "A New Solution of an Eccentric Crack off the Center Line of a Rectangular Sheet for Mode-III", *Engineering Fracture Mechanics*, Vol. 40, pp. 1–7, 1991, https://doi.org/10.1016/0013-7944(91)90120-P.

[13] A. M. Mirzaei, B. Bahrami, and M. R. Ayatollahi, "Asymptotic Stress Field around the Blunt and Sharp Notches in Bimaterial Media under Mixed Mode I/II Loading", *Applied Mathematical Modelling*, Vol. 109, pp. 848–863, 2022, https://doi.org/10.1016/j.apm.2022.04.017.

[14] B. Bahrami, M. R. Ayatollahi, S. K. Alavi, and L. F. M. DaSilva, "On the Prediction of the Stress Field in Adhesive Joints using a Combined Analytical-numerical Method", *International Journal of Adhesion and Adhesives*, Vol. 116, pp. 103151, 2022, https://doi.org/10.1016/j.ijadhadh.2022.103151.

[15] X. F. Li, and K. Y. Lee, "Electroelastic Behavior of a Rectangular Piezoelectric Ceramic with an Antiplane Shear Crack at an Arbitrary Position", *European Journal of Mechanics-A/Solids*, Vol. 23, pp. 645–658, 2004, https://doi.org/10.1016/j.euromechsol.2004.02.004.

[16] T. Yu, T. Q. Bui, P. Liu, C. Zhang, and S. Hirose, "Interfacial Dynamic Impermeable Cracks Analysis in Dissimilar Piezoelectric Materials under Coupled Electromechanical Loading with the Extended Finite Element Method", *International Journal of Solids and Structures*, Vols. 67-68, pp. 205–218, 2015, https://doi.org/10.1016/j.ijsolstr.2015.03.037.

[17] G. Pamnani, S. Bhattacharya, and S. Sanyal, "Analysis of Interface Crack in Piezoelectric Materials using Extended Finite Element Method", *Mechanics of Advanced Material and Structures*, Vol. 26, pp. 1447–1457, 2018, https://doi.org/10.1080/15376494.2018.1432817.

[18] R. T. Faal, and A. A. Dehghan, "Mode III Stress Intensity Factors for Cracked FGM Rectangular Plane", *Engineering Fracture Mechanics*, Vol. 140, pp. 17–30, 2015, https://doi.org/10.1016/j.engfracmech.2015.03.046.

[19] Y. Gu, M. V. Golub, and C. M. Fan, "Analysis of In-plane Crack Problems using the Localized Method of Fundamental Solutions", *Engineering Fracture Mechanics*, Vol. 256, pp. 107994, 2021, https://doi.org/10.1016/j.engfracmech.2021.107994.

[20] B. Abazadeh, and M. Samadi Darafshani, "Mode III Analysis of a Piezoelectric Rectangular Plane Weakened by Multiple Cracks and Cavities", *Theoretical Applied Fracture Mechanics*,Vol. 119, pp. 103366, 2022, https://doi.org/10.1016/j.tafmec.2022.103366.

[21] M. Ayatollahi, M. Abdel-Wahab, and S. M. M. Hashemi, "Transient Analysis of a Cracked Functionally Graded Magneto-electro-elastic Rectangular Finite Plane under Anti-plane Mechanical and In-plane Electric and Magnetic Impacts", *Fatigue and Fracture and Engineering Materials and Structures*, Vol. 47, pp. 220–239, 2023, https://doi.org/10.1111/ffe.14174.

[22] D. A. Hills, P. A. Kelly, D. N. Dai, and A. M. Korsunsky, "*Solution of Crack Problems: The Distributed Dislocation Technique*", Kluwer Academic Publishers, Groningen, 1996, https://doi.org/10.1007/978-94-015-8648-1.

[23] F. Erdogan, and G. D. Gupta, "On the Numerical Solution of Singular Integral Equations", *Quarterly of Applied Mathematics*, Vol. 29, pp. 525–534, 1972, https://www.jstor.org/stable/45340623.

[24] A. M. Cohen, "*Numerical Methods for Laplace Transform Inversion*", Springer Science & Business Media, New York, Vol. 5, 2007, https://doi.org/10.1007/978-0-387-68855-8.

[25] X. S. Zhang, and S. W. Ma, "Transient Response of a Finite Crack in a Rectangular Plate with Stress-free Edges for the Tearing Mode", *Engineering Fracture Mechanics*, Vol. 24, pp. 169–176, 1986, https://doi.org/10.1016/0013-7944(86)90049-4.

[26] A. D. Bykhovski, B. L. Gelmont, and M. S. Shur, "Elastic Strain Relaxation and Piezo Effect in GaN-AlN, GaN-AlGaN, and GaN-InGaN Superlattices", *Journal of Applid Physics*, Vol. 81, pp. 6332–6338, 1997, https://doi.org/10.1063/1.364368.

Appendix

The coefficients in Eq. (8) are,

$$A_{n1}=-\frac{e^{\lambda_n^{(1)}h_2}(1-e^{-2\lambda_n^{(1)}h})\Psi_n}{(1+e^{-2\lambda_n^{(1)}h})}[(\frac{\gamma^{(2)}\lambda_n^{(2)}\Theta_{4n}(1+e^{-2\lambda_n^{(2)}h_2})}{(1-e^{-2\lambda_n^{(2)}h_2})}+\alpha^{(2)}\Theta_{2n})b_{wz}(s)-\Theta_{2n}b_{\varphi z}(s)], \quad (1)$$

$$B_{n1}=\Psi_n e^{\lambda_n^{(1)}h_2}[(\frac{\gamma^{(2)}\lambda_n^{(2)}\Theta_{4n}(1+e^{-2\lambda_n^{(2)}h_2})}{(1-e^{-2\lambda_n^{(2)}h_2})}+\alpha^{(2)}\Theta_{2n})b_{wz}(s)-\Theta_{2n}b_{\varphi z}(s)], \quad (2)$$

$$C_{n1}=\frac{e^{\beta_n h_2}\Psi_n\sinh(\beta_n h)}{\cosh(\beta_n h)}[(\frac{\gamma^{(2)}\lambda_n^{(2)}\Theta_{3n}(1+e^{-2\lambda_n^{(2)}h_2})}{(1-e^{-2\lambda_n^{(2)}h_2})}+\alpha^{(2)}\Theta_{1n})b_{wz}(s)-\Theta_{1n}b_{\varphi z}(s)], \quad (3)$$

$$D_{n1}=-\Psi_n e^{\beta_n h_2}[(\frac{\gamma^{(2)}\lambda_n^{(2)}\Theta_{3n}(1+e^{-2\lambda_n^{(2)}h_2})}{(1-e^{-2\lambda_n^{(2)}h_2})}+\alpha^{(2)}\Theta_{1n})b_{wz}(s)-\Theta_{1n}b_{\varphi z}(s)], \quad (4)$$

$$A_{n2}=0, C_{n2}=0, \quad (5)$$

$$B_{n2}=-\frac{\Psi_n(1-e^{-2\lambda_n^{(1)}h_1})}{(1+e^{-2\lambda_n^{(1)}h})(1-e^{-2\lambda_n^{(2)}h_2})}[\frac{(\gamma^{(2)}\lambda_n^{(2)}\Theta_{4n}(1+e^{-2\lambda_n^{(2)}h_2})+\alpha^{(2)}\Theta_{2n}(1-e^{-2\lambda_n^{(2)}h_2}))b_{wz}(s)}{(1-e^{-2\lambda_n^{(2)}h_2})}$$
$$-b_{\varphi z}(s)]+\frac{e^{-\lambda_n^{(2)}h_2}b_{wz}(s)}{(1-e^{-2\lambda_n^{(2)}h_2})}\frac{\sin(\beta_n\zeta)}{\beta_n}, \quad (6)$$

$$D_{n2}=-\frac{2\varepsilon_{11}^{(1)}(1+e^{-2\beta_n h_1})e^{-\beta_n h_2}\Psi_n}{\varepsilon_{11}^{(2)}(1+e^{-2\beta_n h})(1+e^{-2\beta_n h_2})}[(\frac{\gamma^{(2)}\lambda_n^{(2)}\Theta_{3n}(1+e^{-2\lambda_n^{(2)}h_2})+\alpha^{(2)}\Theta_{1n}(1-e^{-2\lambda_n^{(2)}h_2})}{(1-e^{-2\lambda_n^{(2)}h_2})})$$
$$\times b_{wz}(s)-\Theta_{1n}b_{\varphi z}(s)], \quad (7)$$

where

$$\Theta_{1n}=\frac{\gamma^{(1)}\lambda_n^{(1)}(1+e^{-2\lambda_n^{(1)}h_1})(1-e^{-2\lambda_n^{(2)}h_2})+\gamma^{(2)}\lambda_n^{(2)}(1-e^{-2\lambda_n^{(1)}h_1})(1+e^{-2\lambda_n^{(2)}h_2})}{(1+e^{-2\lambda_n^{(1)}h})(1-e^{-2\lambda_n^{(2)}h_2})}$$

$$\Theta_{2n}=\beta_n(e_{15}^{(1)}-e_{15}^{(2)}\frac{\varepsilon_{11}^{(1)}}{\varepsilon_{11}^{(2)}})\frac{(1+e^{-2\beta_n h_1})}{(1+e^{-2\beta_n h})}$$

$$\Theta_{3n}=(\alpha^{(1)}-\alpha^{(2)})\frac{(1-e^{-2\lambda_n^{(1)}h_1})}{(1+e^{-2\lambda_n^{(1)}h})}$$

$$\Theta_{4n}=\frac{\varepsilon_{11}^{(2)}(1+e^{-2\beta_n h_2})(1-e^{-2\beta_n h_1})+\varepsilon_{11}^{(1)}(1+e^{-2\beta_n h_1})(1-e^{-2\beta_n h_2})}{\varepsilon_{11}^{(2)}(1+e^{-2\beta_n h})(1+e^{-2\beta_n h_2})} \quad (8)$$

and

$$\Psi_n=\frac{\sin(\beta_n\zeta)}{\beta_n(\Theta_{1n}\Theta_{4n}-\Theta_{2n}\Theta_{3n})} \quad (9)$$